Intramolecular Electronic Interactions in Conjugated Ferrocene−π-Extended-Tetrathiafulvalene Donor-π-Donor Molecular Hybrids

Sheng-Gao Liu,† Ignacio Pérez,‡ Nazario Martín,*,‡ and Luis Echegoyen*,†

Department of Chemistry, University of Miami, Coral Gables, Florida 33124, and Departamento de Química Orgánica, Facultad de Ciencias Químicas, Universidad Complutense, E-28040-Madrid, Spain

nazmar@eucmax.sim.ucm.es

Received July 28, 2000

The synthesis of new hybrid ferrocene and π-extended tetrathiafulvalene (TTF) donor[1]-π-donor[2] molecular assemblies **16a**−**c** has been carried out by a Wittig−Horner reaction of the respective phosphonate esters **15a**−**c** with 2-(2-ferrocenylvinyl)-9,10-anthraquinone (**18**) prepared by olefination of ferrocenecarboxaldehyde (**14**) and the anthraquinone phosphonium salt **17**. Electrochemical studies show that the D^1-π-D^2 (D = donor) molecular assemblies **16a**−**c** essentially retain the redox characteristics of both ferrocene and the π-extended TTF components and the effects of solvent, temperature, scan rate, and working electrode are significant. Most importantly, pronounced intramolecular electronic interactions between the two donor moieties were observed by cyclic voltammetry and Osteryoung square wave voltammetry in both the ground and charged states. Semiempirical calculations support the electrochemical observations.

Introduction

The chemistry and properties of the 1,3-dithiole ring has received a lot of attention as a consequence of its interesting redox properties and the ability of the sulfur atoms to engage in intermolecular interactions in the solid state. Tetrathiafulvalene (TTF), bearing two 1,3-dithiole rings in conjugation, and its derivatives (**1**) have been the most intensely studied electron-donor molecules since the discovery of electrical conductivity in the charge-transfer complex between TTF and the electron-acceptor tetracyano-*p*-quinodimethane (TCNQ, **2**).[1] The large number of TTF derivatives synthesized is in contrast to the quite limited number of π-extended TTFs (exTTFs) in which the 1,3-dithiole rings are connected through a conjugating spacer group (**3**) or a *p*-quinodimethane moiety (**4**) (Chart 1),[2] which are versatile building blocks in supramolecular and materials chemistry.[3] Most recently, chemical functionalization of compound **4** has received considerable attention[4,5] and has resulted in several interesting classes of materials.

Systems such as conjugated donor−π-acceptor (D−π-*A*) dyad **5** exhibiting nonlinear optical (NLO) properties and dithia-crown ether annelated exTTF **6** (Chart 1) showing metal ion recognition properties were recently reported by us[6] and Bryce et al.,[7] respectively. Other systems such as **7** and **8** (Chart 2) in which exTTF was directly connected via σ bond(s) to the well-known electron acceptor C_{60} have also been recently reported.[8,9] Most interestingly, in search of new and more sophisticated exTTF derivatives as strong electron donors and potential candidates for the study of intramolecular electronic interactions, multicomponent molecular assemblies **9**−**12** (Chart 3) in which the donor moieties were linked by a σ bond forming D−σ-D or D^1−σ-D^2 or D^1−σ-D^2−σ-D^1 dyads or triads have been reported.[3b,c,10,11] In these systems, such as the first exTTF dimer **9**,[3b,c] no intramolecular electronic interactions were observed.[3b,c] This results from the lack of conjugation between the two donor moieties.[3b,10−12] Most recently, we have shown that weak intramolecular electronic interactions occur between the TTF and exTTF when they are connected through a conjugating spacer as in compound **13**.[13] These

† University of Miami.
‡ Universidad Complutense.

(1) (a) Ferraris, J.; Cowan, D. O.; Walatka, V. V.; Perlstein, J. H. *J. Am. Chem. Soc.* **1973**, *95*, 948. (b) Coleman, L. B.; Cohen, M. J.; Sandman, D. J.; Yamagishi, F. G.; Garito, A. F.; Heeger, A. J. *Solid State Commun.* **1973**, *12*, 1125.

(2) Martín, N.; Ortí, E. Quinonoid π-extended TTFs. In *Handbook of Advanced Electronic and Photonic Materials*; Nalwa, N. S., Ed.; Academic Press: New York, 2001; Vol. 3, Chapter 6, pp 245−265.

(3) (a) Bryce, M. R.; Moore, A. J.; Hasan, M.; Ashwell, G. J.; Raser, A. T.; Clegg, W.; Hursthouse, B.; Karaulov, A. I. *Angew. Chem., Int. Ed. Engl.* **1990**, *29*, 1450. (b) Martín, N.; Pérez, I.; Sánchez, L.; Seoane, P. *J. Org. Chem.* **1997**, *62*, 870. (c) Martín, N.; Pérez, I.; Sánchez, L.; Seoane, P. *Synth. Met.* **1997**, *86*, 1867. (d) Martín, N.; Sánchez, L.; Seoane, C.; Ortí, E.; Viruela, P. M.; Viruela, R. *J. Org. Chem.* **1998**, *63*, 1268. (e) Yamashita, Y.; Tomura, M. *J. Mater. Chem.* **1998**, *8*, 1933. (f) Boulle, C.; Desmars, O.; Gautier, N.; Hudhomme, P.; Cariou, M.; Gorges, A. *Chem. Commun.* **1998**, 2197. For a recent review on functionalized TTFs with potential applications as versatile π-electron systems in materials chemistry, see: Bryce, M. R. *J. Mater. Chem.* **2000**, *10*, 589.

(4) (a) Bryce, M. R.; Finn, T.; Moore, A. J. *Tetrahedron Lett.* **1999**, *40*, 3271. (b) Bryce, M. R.; Finn, T.; Moore, A. J.; Batsanov, A. S.; Howard, J. A. K. *Eur. J. Org. Chem.* **2000**, 51.

(5) For a recent review on *o*-quinodimethanes, see: Segura, J. L.; Martín, N. *Chem. Rev.* **1999**, *99*, 3199.

(6) Herranz, M. A.; Martín, N:; Sánchez, L.; Garín, J.; Orduna, J.; Alcalá, R.; Villacampa, B.; Sánchez, C. *Tetrahedron* **1998**, *54*, 11651.

(7) Bryce, M. R.; Batsanov, A. S.; Finn, T.; Hanse, T. K.; Howard, J. A. K.; Kamenjicki, M.; Lednev, I. K.; Asher, S. A. *Chem. Commun.* **2000**, 295.

(8) (a) Martín, N.; Sánchez, L.; Guldi, D. M. *Chem. Commun.* **2000**, 113. (b) Martín, N.; Pérez, I.; Sánchez, L.; Seoane, C. *J. Org. Chem.* **1997**, *62*, 5690.

(9) (a) Christensen, C. A.; Bryce, M. R.; Batsanov, A. S.; Howard, J. A. K.; Jeppesen, J. O.; Becher, J. *Chem. Commun.* **1999**, 2433. (b) Herranz, M. A.; Martín, N. *Org. Lett.* **1999**, *37*, 5690.

(10) Cerrada, E.; Bryce, M. R.; Moore, A. J. *J. Chem. Soc., Perkin Trans. 1* **1993**, 537.

(11) Marshallsay, G.; Bryce, M. R. *J. Org. Chem.* **1994**, *59*, 6847.

10.1021/jo001149w CCC: $19.00
Published on Web 12/06/2000

Chart 1

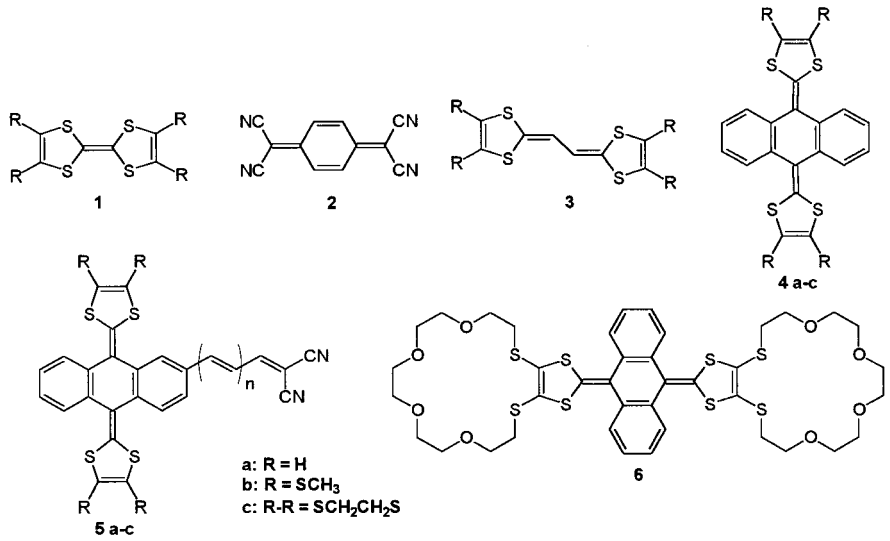

Chart 2

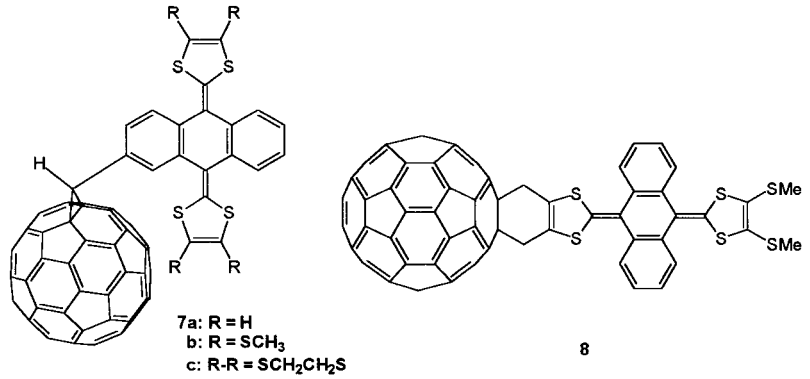

findings prompted us to synthesize and investigate the electronic interactions for the new multicomponent electron donor systems **16** in which the exTTF is covalently attached in conjugation to another strong electron donor ferrocene[14] through a vinyl spacer. The advantage of using ferrocene instead of TTF is that ferrocene has only a single one-electron redox process at potentials near to the first oxidation of TTF. Furthermore, the oxidation potential of its derivatives FcX [where Fc denotes the ferrocenyl group Fe(η^5-C_5H_5)(η^5-C_5H_4)], especially those in which the bonded α-carbon is sp^2 hybridized, is much more sensitive to the effect of the substituent than when the substituent is bonded to the cyclopentadienyl ring through a sp^3 carbon atom.[15] This should enable us to more easily and conveniently study the electronic interactions between the two donor moieties in the ground as well as in the charged states with respect to compound **13**.[13]

Results and Discussion

Synthesis. Preparation of the target compounds **16a**−**c** was carried out as described in Scheme 1. Thus the olefination Wittig reaction between commercially available formylferrocene **14** and triphenylphosphonium bromide **17**[16] afforded, under different basic conditions (*n*-BuLi/THF, Δ or NaOH/CH_2Cl_2), a mixture of the *Z* (**18**, vinyl protons at $\delta = 6.5$ and 6.8 ppm, $J \approx 12$ Hz) and *E* (**18**, vinyl protons at $\delta = 6.8$ and 7.2 ppm, $J \approx 16$ Hz) isomers of the 2-(2-ferrocenylvinyl)-9,10-anthraquinone in a moderate yield (42%) when using *n*-BuLi as the base and in very poor yield (5%) when NaOH was used as the base. The resulting isomeric mixture was easily isomerized to the *E* isomer **18** by refluxing in xylene in the presence of iodine. However, when the reaction between **14** and **17** was carried out using potassium *tert*-butoxide as the base in refluxing toluene, only the *E* isomer was obtained in 90% yield (see Experimental Section). Compound **18** exhibits a violet color and its UV−Vis spectrum in methanol shows the presence of a low energy broad wave at $\lambda_{max} = 535$ nm ($\log\epsilon = 3.64$) which can be accounted for as an intramolecular charge transfer (ICT) band resulting from the strong electron donor ferrocene and the electron acceptor anthraquinone moiety (see below).

(12) Bryce et al. hinted that inter- or intramolecular electronic interactions may exist in systems **11** and **12**; however, no convincible evidence were presented.[11]

(13) Pérez, I.; Liu, S. G.; Martín, N.; Echegoyen, L. *J. Org. Chem.* **2000**, *65*, 3796.

(14) Ferrocene is a well-known electron donor molecule which, similarly to TTF, has been successfully used in supramolecular and materials chemistry, see: Togni, A. Ferrocene-Containing Charge-Transfer Complexes. Conducting and Magnetic Materials. In *Ferrocenes*; Togni, A., Hayashi, T., Ed.; VCH: Weinheim, 1995.

(15) Silva, M. E. N. P. R. A.; Pombeiro, A. J. L.; Fraústo da Silva, J. J. R.; Herrmann, R.; Deus, N.; Bozak, R. E. *J. Organomet. Chem.* **1994**, *480*, 81.

(16) (a) Newell, A. K.; Utley, J. H. P. *J. Chem. Soc, Chem. Commun* **1992**, 800. (b) Listvam, V. N.; Stasyunk, A. P. *Zh. Obshch. Khim.* **1985**, *55*, 756.

Chart 3

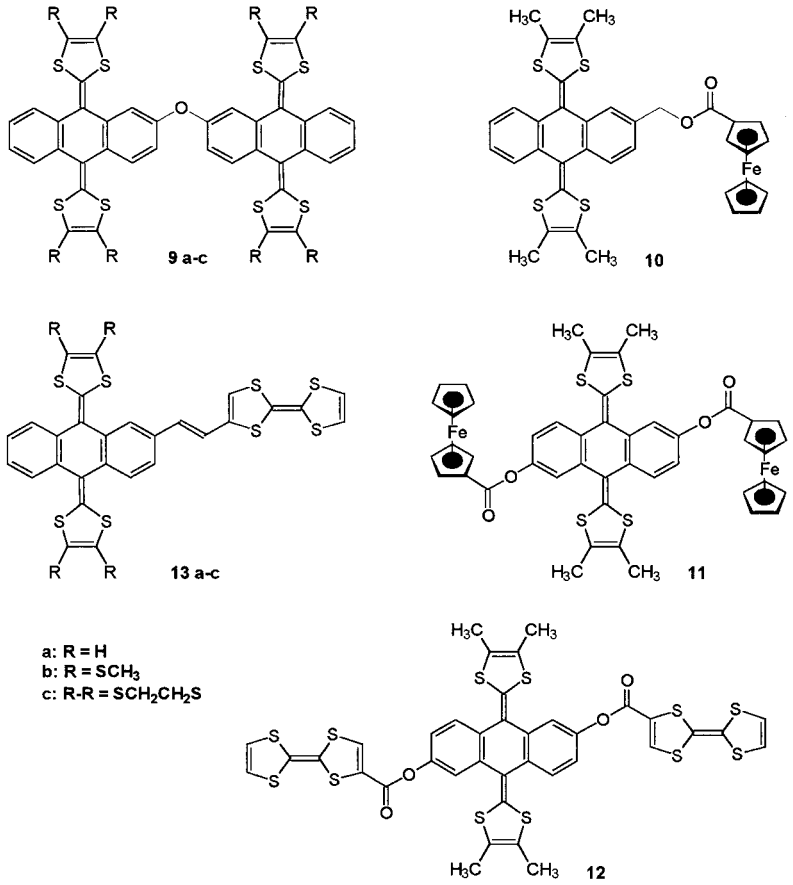

Scheme 1. Synthetic Procedures for Compounds 16

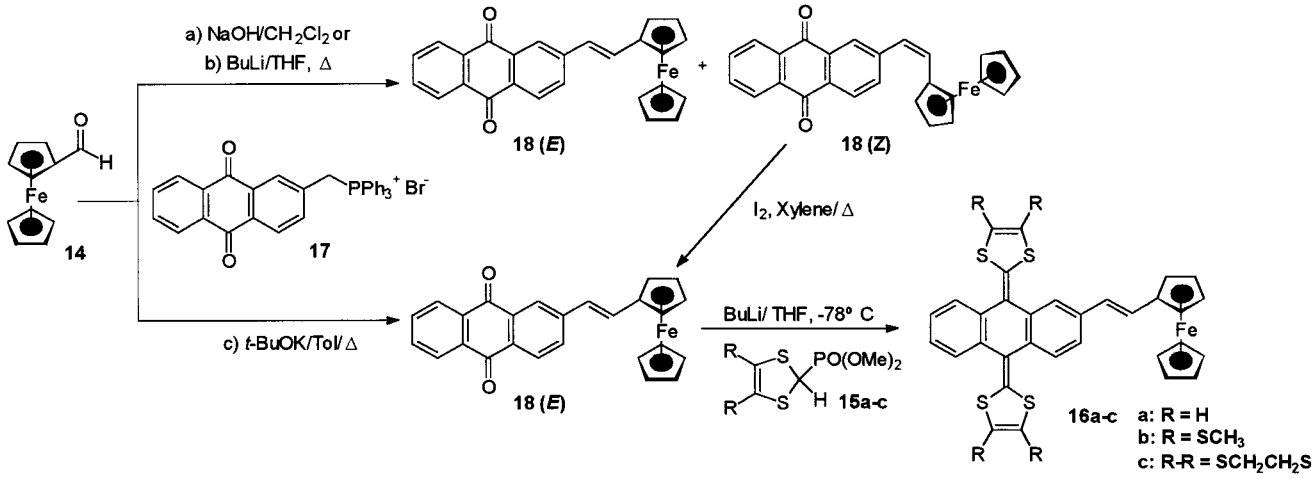

Finally, the target molecules **16a**−**c** were synthesized from **18** by employing the Wittig−Horner olefination reaction with the carbanion generated from the respective phosphonate esters **15a**−**c** in the presence of *n*-BuLi at −78 °C. The starting phosphonates **15a**−**c** were in turn prepared using a multistep synthetic procedure as previously described in the literature.[17] The new electron donor assemblies **16a**−**c** were purified by flash-chromatrogaphy on silica gel using hexane:dichloromethane (1:2 v/v) as the eluent and obtained as orange stable solids in moderate yields (59−64%).

(17) (a) Bryce, M. R.; Moore, A. J. *Synthesis*, **1991**, 26. (b) Parg, R. P.; Kilburn, J. D.; Ryan, T. G. *Synthesis* **1994**, 195 and references therein.

The ^{1}H NMR spectra of dyads **16a**−**c** show, in addition to the expected aromatic signals for the ferrocene and anthracene moieties, the presence of the vinyl protons as two doublets at $\delta \approx 6.7$ and 6.9 ppm with coupling constants of $J \approx 16$ Hz, thus confirming the *E* isomeric structure.

Electrochemistry. Effects of Solvent, Temperature, and Working Electrodes. Redox properties of **16a**−**c** on different electrodes (platinum, gold, and glassy carbon (GC)) were studied by cyclic voltammetry (CV) and Osteryoung square wave voltammetry (OSWV) at ambient temperature (20 °C) and at 0 °C in different solvents (THF, CH_2Cl_2, and CH_3CN) using tetrabutylammonium hexafluorophosphate ($TBAPF_6$) as the support-

Table 1. $E_{1/2}$[a] and/or E_{pa} Values (mV vs Ag/AgCl) of Compounds 16a−c, 4a−c, and Ferrocene detected by CV in different solvents at ambient temperature on platinum, gold, and glassy carbon (GC) electrode. v=100 mV s^{-1}. Errors for E_{pa} or $E_{1/2}$ values are estimated at about ±5 mV

	E_{pa}[b]					$E_{1/2}$ (ΔE_p/mV)				
	THF	CH_2Cl_2		CH_3CN		THF	CH_2Cl_2		CH_3CN	
compd	Pt	Pt	Pt	Au	GC	Pt	Pt	Pt	Au	GC
4a	537[13]	469[c]	365	342	404			*d*	309 (66)	*d*
4b	680[13]	562			466[f]			*e*	*e*	*e*
4c	642[c, 13]	517[c]	468	474	456			*d*	*d*	422 (67)
ferrocene	615	504	486	488	483	584 (63)	475 (59)	448 (56)	448 (60)	447 (57)
16a	501, 570	341[c]	342, 537	337, 539	320, 531	547 (47)[g]	*c*	514 (45)[g]	514 (51)[g]	508 (46)[g]
16b	598	449			419, 531[f]		419 (60)	*e*	*e*	*e*
16c	592	423	416, 510[f]	414, 510[f]	412, 504[f]		392 (62)	*d*	*d*	502 (43)[g]

[a] $E_{1/2} = (E_{pa} + E_{pc})/2$, E_{pa} or E_{pc}: peak potentials, $\Delta E_p = E_{pa} - E_{pc}$; reported for reversible redox processes only. [b] Peak potentials reported, due to electrochemical or chemical irreversibility. [c] Only one chemically irreversible oxidation peak observed under this condition. [d] Ir-reversible at 100 mV s^{-1} (ΔE_p > 70 mV). [e] Solubility in CH_3CN is very low and thus it is difficult to record CVs. [f] OSWV values due to low solubility. [g] $E_{1/2}$ and ΔE_p values for the ferrocene-based redox process only.

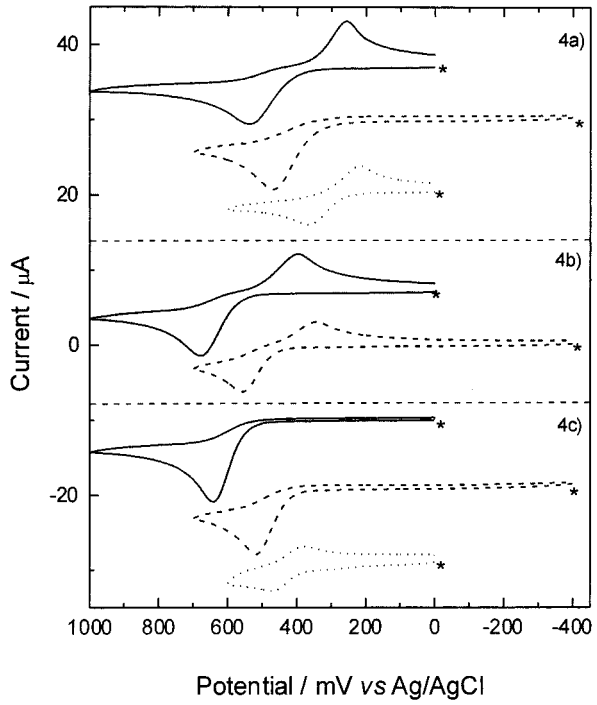

Figure 1. CVs of **4a**−**c** in THF (solid), CH_2Cl_2 (dashed), and CH_3CN (dotted) at ambient temperature on a Pt electrode at 100 mV s^{-1}. * sweep starting point.

ing electrolyte in 0.1 mol L^{-1} concentration. The electrochemical data recorded at ambient temperature using different electrodes and solvents are summarized in Table 1 along with those of the model exTTFs **4a**−**c** and ferrocene for comparison.

Generally speaking, unlike TTF, exTTFs **4a**−**c** exhibit a single two-electron chemically reversible (sometimes irreversible) oxidation process to form a dicationic state in the solvents tested.[3b,13,18] As shown in Figure 1, in both THF[13] and CH_2Cl_2, compound **4c** showed only one oxidation wave without any associated reduction peaks in the reverse scan on Pt, Au, or GC electrodes. On the other hand, **4b** showed a chemically reversible but electrochemically irreversible redox wave with peak-to-peak potential separation ($\Delta E_p = E_{pa} - E_{pc}$) values of 211 and 285 mV (v = 100 mV s^{-1} on a Pt electrode) in CH_2Cl_2 and THF, respectively. **4a** in THF behaved similar to **4b**, showing an electrochemically irreversible redox wave with ΔE_p = 275 mV (v = 100 mV s^{-1} on a Pt electrode),[13] but in CH_2Cl_2 it showed only one chemically irreversible oxidation wave like **4c**. However, in CH_3CN, **4a**−**c** showed an oxidation wave with an associated reduction peak in the reverse scan on Pt, Au, or GC electrodes.[19] Furthermore, for all the cases, both the oxidation peak potential ($\mathbf{E}_{pa}$) and the ΔE_p values (if observed) in CH_3CN are generally less than those in either THF or CH_2Cl_2 and those in CH_2Cl_2 are generally less than those in THF (CH_3CN < CH_2Cl_2 < THF) with the same working electrode at scan rates from 20 to 600 mV s^{-1}. Using different electrodes, both the E_{pa} and the ΔE_p values generally follow the trend GC > Pt > Au in the case of **4a**, but the trend is reversed for **4c**. In addition, both the E_{pa} and E_{pc} (the rereduction peak potential) values are a function of the scan rate and temperature. For **4a**−**c**, increasing the scan rate or lowering the temperature results in a significant increase of the E_{pa} and a decrease of the E_{pc} values, indicative of a slow heterogeneous electron-transfer process.[3,13] Therefore, the overall effect of lowering the temperature and increasing the scan rate significantly increases the ΔE_p values. In addition, as can be seen in Table 1, the E_{pa} value of **4b** is generally larger than that of **4c**, and that of **4c** is larger than for **4a** in all the solvents tested under similar conditions, showing the trend **4b** > **4c** > **4a**. Therefore, considering all variables, only **4a** on gold and **4c** on glassy carbon exhibited a single well-behaved, diffusion-controlled, electrochemically reversible, two-electron oxidation process at ambient temperature at very slow scan rates, shown in Figure 2. To our knowledge, this is the first time that an electrochemically reversible redox process is observed for exTTF analogues **4**. It is important to note that both ferrocene and TTF showed typical diffusion-controlled electrochemically reversible redox process(es) with redox potentials independent of scan rate and working electrode, but dependent on the solvent as for **4a**−**c** (E_p or $E_{1/2}$ values of ferrocene in the different solvents follow the same trend as those of **4a**−**c**, i.e., THF > CH_2Cl_2 > CH_3CN, Table 1). The temperature effects on the electrochemical properties of ferrocene are not as significant as for **4a**−**c**.

Compounds **16a**−**c** also show some common features such as **4a**−**c** and pronounced solvent, temperature, working electrode and scan rate effects. In CH_2Cl_2 on a

(18) Moore, A. J.; Bryce, M. R. *J. Chem. Soc., Perkin Trans. 1* **1991**, 157.

(19) Solubility of **4b** in CH_3CN is too low to record a satisfied CV under consistent conditions as of **4a** and **4c**; however, a weak oxidation and the rereduction peaks were observed by OSWV.

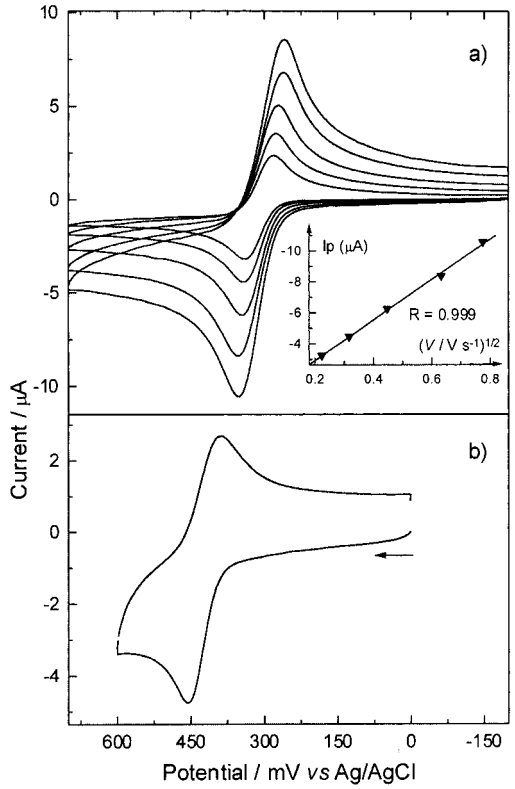

Figure 2. CVs of (a) **4a** on a gold electrode (20−600 mV s^{-1}) and (b) **4c** (100 mV s^{-1}) on a glassy carbon in CH_3CN at ambient temperature. Inset of (a): I_p vs $V^{1/2}$ showing a diffusion-controlled process.

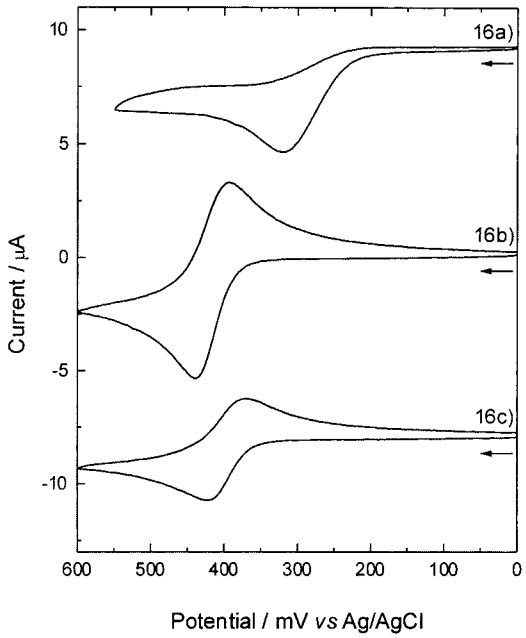

Figure 3. CVs of **16a**−**c** in CH_2Cl_2 at ambient temperature on a Pt electrode. v = 20 mV s^{-1}.

Pt electrode and at ambient temperature, **16a**−**c** showed only one oxidation wave at peak potentials of 341, 449, and 423 mV (v = 100 mV s^{-1}), respectively, with (for **16b**,**c**) or without (for **16a**) an associated reduction peak in the reverse scan (Figure 3). For **16b**,**c**, such a process is electrochemically reversible or quasi-reversible (ΔE_p < 62 mV) at slow scan rates (<100 mV s^{-1}). Both the E_{pa} and ΔE_p values (if observed) increased with the increase of scan rate and a new broad reduction peak was observed at around 200−250 mV in the reverse scan for both compounds **16b**,**c** when increasing the scan rate to about 600−1000 mV s^{-1}.

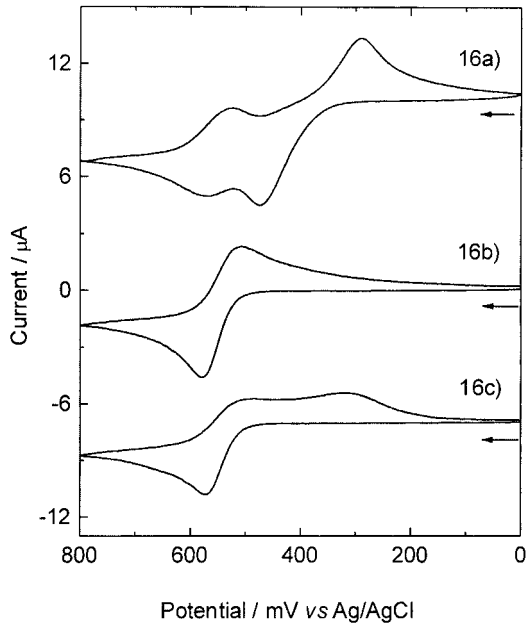

Figure 4. CVs of **16a**−**c** in THF at ambient temperature on a Pt electrode. v = 20 mV s^{-1}.

In THF using Pt, Au, or GC electrodes and at either ambient temperature or 0 °C, **16a** showed two oxidation waves associated with two corresponding reduction peaks in the reverse scan (Figure 4). The ΔE_p values for the second redox process (ΔE_p^2) are generally around 60 mV and are independent of the scan rate and electrode, indicative of a reversible process. For the first redox process, the ΔE_p values are generally larger than 100 mV even at very slow scan rates (v = 20 mV s^{-1}) and are very dependent on the scan rate, temperature, and electrode (Pt > Au > GC), indicative of an electrochemically irreversible process with slow heterogeneous electron-transfer rate. When the scan rate was increased to 400 or 600 mV s^{-1}, the first redox wave overlapped with the second one, resulting in the observation of only one redox peak on Pt, GC or Au electrodes. However, for **16b** and **16c**, only one chemically reversible but electrochemically irreversible (ΔE_p > 70 mV) redox process was observed at either ambient temperature or 0 °C on the three different electrodes, indicating the coalescence of all oxidation processes into one, three-electron process (Figure 4). Also observed is the high dependence of the E_{pa} or ΔE_p values on the scan rate, temperature, and electrode. In addition, similarly to **16b** in CH_2Cl_2, an additional new broad reduction peak at around 310 mV (v = 600 mV s^{-1}) can be observed at higher scan rates in the reverse scan for **16b**. However, in the case of **16c**, two separate reduction peaks are observed as for **16a** even at very slow scan rates (20 mV s^{-1}, Figure 4). It should be mentioned that all our attempts to separate this three-electron oxidation wave into two peaks by changing either the scan rate, temperature, or working electrode were not successful. However, changing the solvent to CH_3CN resulted in such a separation.

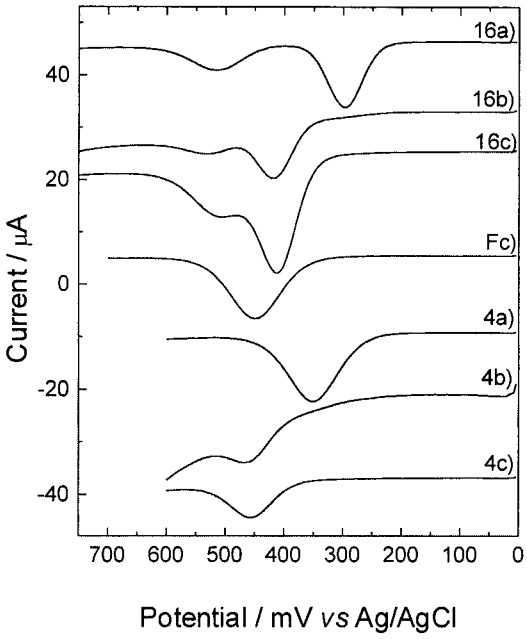

Figure 5. OSWVs of **16a**−**c**, ferrocene, and **4a**−**c** in CH_3CN at ambient temperature on a glassy carbon electrode.

Figure 5 shows the OSWVs of **16a**−**c** in CH_3CN at ambient temperature along with those of **4a**−**c** and ferrocene for comparison. It is very clear that **16a**−**c** showed two well-resolved oxidation processes. The corresponding CVs, shown in Figure 6, show that these electron transfer processes are both chemically and electrochemically reversible or quasi-reversible at slow scan rates. Due to the low solubility of **16b** in CH_3CN (solubility in CH_3CN follows **16a** > **16c** > **16b**, similar to **4a**−**c**), two electrochemically quasi-reversible redox processes were also observed in a 2:1 CH_3CN/CH_2Cl_2 mixed solvent for **16b** at ambient temperature (middle of Figure 6).

Considering the fact that compounds **16a**−**c** contain two different types of donor moieties, it was important to determine which is easier to oxidize. Thus, a careful comparison was made between the electrochemical data of **16a**−**c** and those of ferrocene and exTTFs **4a**−**c** (Figure 5 and Table 1). In CH_3CN, **4a**−**c** are easier to oxidize than ferrocene on all electrodes. On the contrary, in both THF and CH_2Cl_2, ferrocene is easier to oxidize than both **4b** and **4c** (but not **4a**). Therefore, the first oxidation should correspond to the exTTF moiety for **16a**−**c** in CH_3CN and for **16a** in THF. Considering the fact that **4a**−**c** exhibit a single, two-electron oxidation process in both THF and CH_3CN (see above), the first oxidation peak of **16a**−**c** in CH_3CN or **16a** in THF is a two-electron process corresponding to the formation of a dication from the neutral state and the second oxidation process corresponds to the oxidation of the ferrocene moiety by one electron, leading overall to the formation of a tricationic state. This explanation is in good agreement with the fact that the integration of the first oxidation peak for **16a**−**c** in CH_3CN or for **16a** in THF is approximately twice the area of the second oxidation wave. This assignment is also supported by the fact that the first oxidation of **16a**−**c** in CH_3CN or **16a** in THF is electrochemically irreversible, similar to the behavior of **4a**−**c**, and the second is reversible. Furthermore, the redox potentials of this two-electron process are highlyl

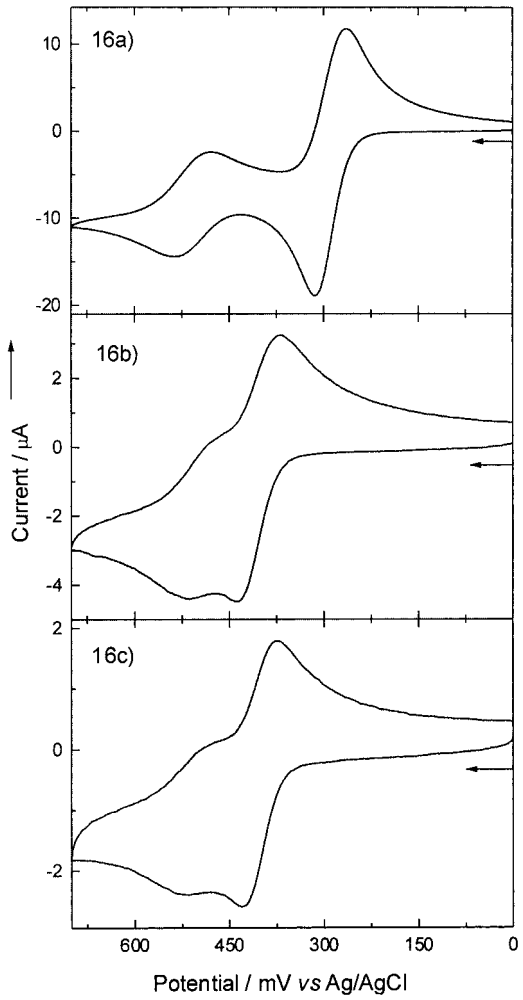

Figure 6. CVs of **16a**,**c** in CH_3CN and **16b** in 2:1 CH_3CN/CH_2Cl_2 on a glassy carbon electrode at ambient temperature. $v = 20$ mV s^{-1}.

scan rate, solvent and electrode dependent, consistent with the behavior of **4a**−**c**, but in contrast to the behavior of ferrocene, for which, the redox potential is almost independent of the scan rate and working electrode (Table 1). However, the second reversible oxidation at ca. 500 mV with small ΔE_p values (≤ 51 mV, $v = 100$ mV s^{-1}) is almost independent of scan rate, temperature (0−20 °C), or working electrode for all the three compounds, consistent with a ferrocene-based redox process. It is also evident that this ferrocene-based reversible oxidation corresponds to a one-electron process when compared to the corresponding oxidation of the parent ferrocene under identical concentration and experimental conditions.

In both CH_2Cl_2 and THF **16b**,**c** exhibit only one oxidation wave due to the coalescence of the two different oxidation processes into one, three-electron process directly leading overall to the formation of a tricationic state Fc^+-$exTTF^{2+}$, as outlined in Scheme 2.

Comparing the redox potential values for **16a**−**c** shows that the first oxidation peak potential (E_{pa}^1) of **16b** in either CH_3CN, THF, or CH_2Cl_2 is more positive than that of **16c**, and that of **16c** is more positive than that of **16a**, following the trend of **16a** < **16c** < **16b**. This is in perfect agreement with the electrochemical data (E_{pa}) of the model exTTFs **4a**−**c** (**4a** < **4c** < **4b**). Thus, the geometric distortion found in the exTTFs **4a**−**c**[3a] could be respon-

Scheme 2 Schematic Diagram of the Redox Processes for Compounds 16a−c. Fc-exTTF Denotes the Fc-π-exTTF as in the Text

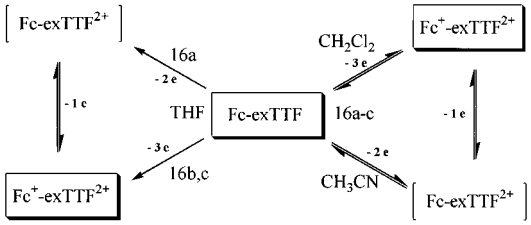

sible for the coalescence of the first and second oxidation processes into a single two-electron oxidation wave to form a planar, aromatic hydrocarbon skeleton in the exTTF moiety of **16a**−**c**.[20] Although the same behavior was observed in THF for compound **16a**, this is not the case for **16b**,**c**, which showed only one three-electron oxidation wave.

Intramolecular Electronic Interactions. When comparing the CVs of the Fc-π-exTTF molecular hybrids **16a**−**c** with those of ferrocene and exTTFs **4a**−**c**, although some common features exist (see above), it is also quite obvious that in each case the CV of the Fc-π-exTTF is not exactly the sum of the CVs of ferrocene and exTTF. This is a good indication of intramolecular electronic interactions between the two donor moieties.

The exTTF-based redox waves of **16a**−**c** is different from that of **4a**−**c** in both shape and peak potential. For example, in both CH_2Cl_2 and THF, **16c** showed one oxidation process with associated reduction peak(s) in the reverse scan, in contrast to **4c**, for which no reduction peaks were observed in both solvents. In contrast, in CH_2Cl_2 **16a** showed only one oxidation peak without any associated reduction detected in the reverse scan on either Pt or GC electrode, but **4a** showed one oxidation with an associated reduction in the back scan on a GC electrode (but not on a Pt electrode). In the case of **16a** in both CH_3CN and THF, both the exTTF-based E_{pa} and ΔE_p (E_{pa}^1 and ΔE_p^1) values generally follow the trend of Pt >Au > GC, but for **4a**, the trend is GC > Pt > Au (CH_3CN). In addition, as can be seen in Figure 5 in CH_3CN, all the Fc-based oxidation waves for **16a**−**c** are more positive than that of the parent ferrocene (448 mV) by 68, 83, and 56 mV (OSWV values) for **16a**, **16b**, and **16c**, respectively. This indicates the existence of intramolecular electronic interactions between the two moieties in the charged states of **16a**−**c**, i.e., when they are oxidized from the neutral to the dicationic state (Fc-π-exTTF^{2+}), oxidation of the Fc moiety becomes more difficult due to the electron withdrawing effect of the dicationic state of the exTTF moiety (exTTF^{2+}). Such an intramolecular electronic interaction was also observed in the ground state. Thus, a comparison of the first oxidation potential (E_{pa}^1) of **16a**−**c** (Fc-π-exTTF → Fc-π-exTTF^{2+}) with those of the model exTTFs **4a**−**c** (Figure 5), reveals that the anodic peak potential differences for **4a**−**16a**, **4b**−**16b**, and **4c**−**16c** are about 48, 47, and 31 mV, respectively. This must result from the conjugation between the two donor moieties. Based on these observations and other reported data,[15] oxidation of the Fc moiety in **16a**−**c** (vinyl ferrocene) should be easier than that of the parent ferrocene.[15] However, when the exTTF moiety was oxidized to the dicationic state, the oxidation of the Fc moiety in **16a**−**c** became more difficult, showing that the inductive effect from the positively charged dicationic state of the exTTF moiety is much more pronounced. This also indicates that the intramolecular electron withdrawing effect from the exTTF^{2+} moiety on the oxidation of the Fc moiety in **16a**−**c** is larger relative to vinyl ferrocene. Such a ground-state intramolecular electronic interaction is in good agreement with the UV−vis spectroscopic analysis. As shown in Figure 7, the UV−vis spectra of **16a**-**c** in CH_3CN are mainly dominated by the absorption of the exTTF moiety in the region of 350−500 nm (in the region of 300−500 nm, no intense absorption was observed for ferrocene, not shown in the figure). Thus, a comparison of the λ_{max} values in the region of 350−400 nm shows a red-shift of 16, 19 and 11 nm and in the region of 400−500 nm, a red shift of 11, 17, and 10 nm was also observed for **16a** vs **4a**, **16b** vs **4b**, and **16c** vs **4c**, respectively. In addition, for the absorption in the region of 400−500 nm, the full width at half-maximum (fwhm) for compounds **16a**−**c** is larger than that of **4a**−**c** by about 17 nm in CH_3CN, indicative of intramolecular electronic interactions.

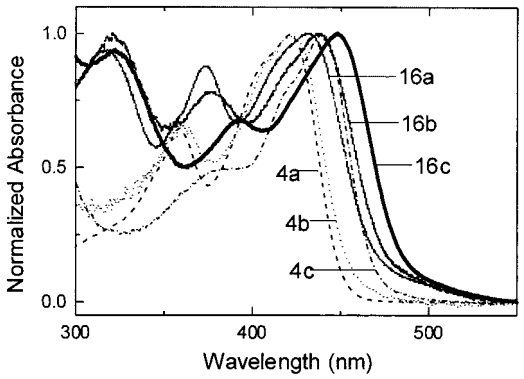

Figure 7. UV−vis of **16a**−**c**, ferrocene, and **4a**−**c** in CH_3CN at ambient temperature.

It should be pointed out that such intramolecular electronic interactions observed in **16a**-**c** are in contrast to the observations for exTTF-σ-exTTF dimer **9**, in which the two donor fragments behave independently, showing a single, four-electron, irreversible redox wave because the two exTTF moieties are connected by two σ bonds via an insulating oxygen atom that inhibits the electronic coupling. However, the intramolecular electronic interactions observed for **16a**−**c** are consistent with the observations for **13**, which showed a small but evident intramolecular electronic interaction between the TTF and the exTTF units across the spacer ethylene bridge.[13]

To rule out the possible effects arising from intermolecular electronic interactions, we studied the electrochemical properties of a mixture of the parent ferrocene and a model exTTF, compound **4a**, in CH_3CN−$TBAPF_6$ at ambient temperature on all three electrodes (Pt, Au, GC). Figure 8 shows the CVs of ferrocene, **4a** and **4a** + ferrocene in CH_3CN on a Pt electrode. It is very clear that the CV of the mixture of **4a**+ferrocene is simply the sum of the constituent CVs (the same phenomena were also observed on Au or GC electrodes), which is very different from that observed for **16a** (see above).

(20) Bryce et al. reported the X-ray analysis of an analogue compound of **4** with R = CH_3, see Chart 1, which was found to show a highly distorted geometry in the neutral state and a planar anthracene moiety with the two 1,3-dithiole rings in almost an orthogonal position (86.0 °C) in the dicationic state.[3a]

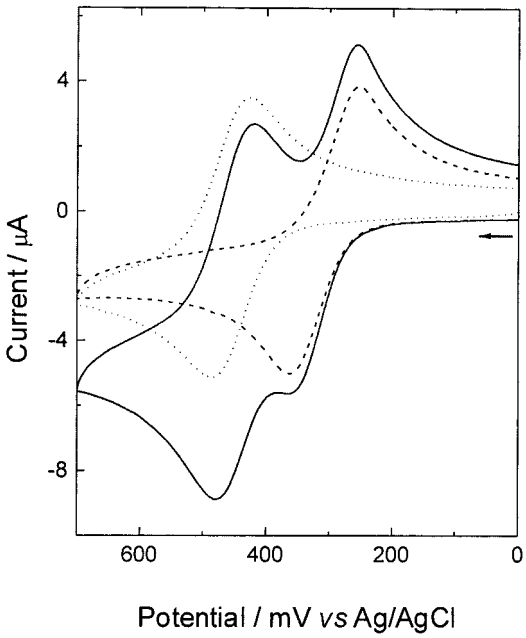

Figure 8. CVs of ferrocene (dotted), **4a** (dashed) and **4a** + ferrocene (solid) in CH_3CN at ambient temperature on a Pt electrode. $v = 100$ mV s^{-1}.

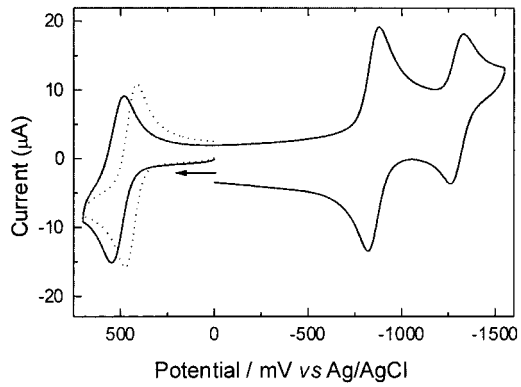

Figure 9. CVs of compound **18** (solid) and ferrocene (dotted) in CH_3CN at ambient temperature on a glassy carbon electrode. $v = 100$ mV s^{-1}.

Such intramolecular electronic interactions observed in these novel D^1-π-D^2 systems **16a**−**c** are comparable with those observed for D-π-A system **18** (Scheme 1), in which an electron donor (ferrocene) and an acceptor (9,10-anthraquinone, AQ) are connected through a C=C double bond forming a Fc-π-AQ dyad. Figure 9 shows the CVs of **18** and the parent ferrocene in CH_3CN on a glassy carbon electrode. Both the one-electron characteristic oxidation wave from the Fc moiety and the two, one-electron reduction waves from the AQ unit are clearly observed for **18**. The reduction processes are characteristic of AQs in organic solution,[21−26] and the CV exhibited

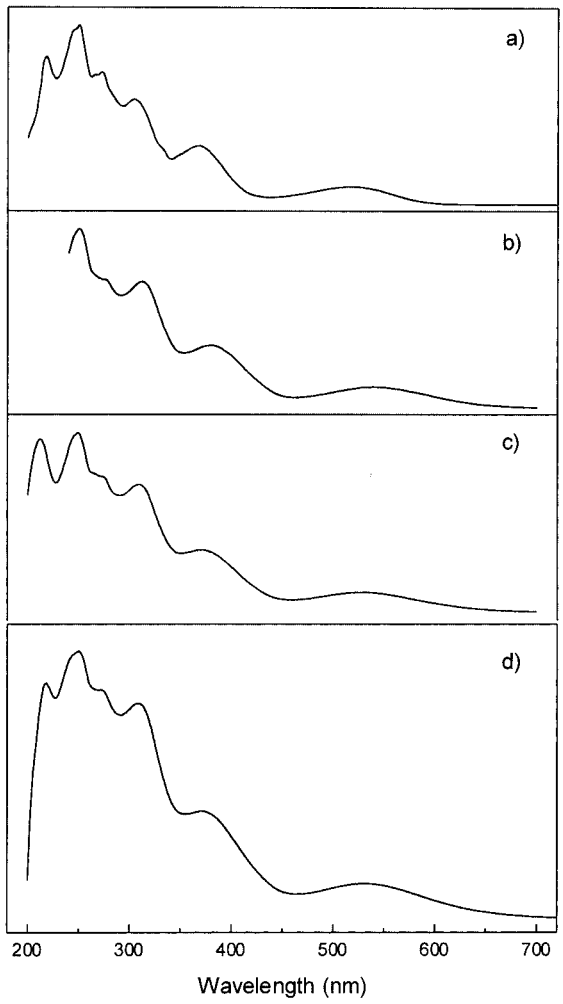

Figure 10. Normalized UV−vis absorption spectra of **18** in (a) cyclohexane, (b) dichloromethane, (c) acetonitrile, and (d) methanol. The vertical axis represents the absorbance.

the usual two electrochemically reversible waves ($E_{1/2}^1 = -850$ mV with $\Delta E_p = 55$ mV and $E_{1/2}^2 = -1302$ mV with $\Delta E_p = 60$ mV at 100 mV s^{-1}) corresponding to the two, one-electron-transfer processes leading to the formation of a dianionic anthraquinone, AQ^{2-}. Most importantly, comparison of the oxidation potential of the Fc moiety in **18** with that of the parent ferrocene shows a significant positive shift of 73 mV. It must be pointed out that attaching a vinyl group to ferrocene has a negligible effect on its redox potential,[15] so the shift observed here must result from the attached anthraquinone group. Since no potential shifts were detected for mixtures of AQ and ferrocene under similar conditions, this anodic shift of the Fc unit in **18** must reflect an intramolecular D−A interaction. Such intramolecular electronic interaction is supported by the electronic absorption spectra. As shown in Figure 10, the absorption profile of the Fc-π-AQ comprised a set of peaks in the UV region at wavelengths < 450 nm and a broad, low-energy band in the visible region at around 530 nm. This visible absorption band can be assigned to an ICT transition, similar to those observed for single component highly conjugated rigid D-π-A systems previously reported by our group and Bryce et al.[27]

(21) Chen, Z.; Schall, O. F.; Alcala, M.; Li, Y.; Gokel, G. W.; Echegoyen, L. *J. Am Chem. Soc.* **1992**, *114*, 444.
(22) Echegoyen, L.; Lawson, R. C.; Lopez, C.; de Mendoza, J.; Hafez, Y.; Torres, T. *J. Org. Chem.* **1994**, *59*, 3814.
(23) Echegoyen, L.; Hafez, Y.; Lawson, R. C.; de Mendoza, J.; Torres, T. *Tetrahedron Lett.* **1994,** *35*, 6383.
(24) Echegoyen, L.; Gustowski, D. A.; Gatto, V. J.; Gokel, G. W. *J. Chem. Soc., Chem. Commun.* **1986,** 220.
(25) Kaifer, A.; Gustowski, D. A.; Echegoyen, L.; Gatto, V. J.; Schultz, R. A.; Cleary, T. P.; Morgan, C. R.; Goli, D. M.; Rios, A. M.; Gokel, G. W. *J. Am. Chem. Soc.* **1985,** *107*, 1958.
(26) Gustowski, D. A.; Echegoyen, L.; Goli, D. M.; Kaifer, A.; Schultz, R. A.; Gokel, G. W. *J. Am. Chem. Soc.* **1984,** *106*, 1633.

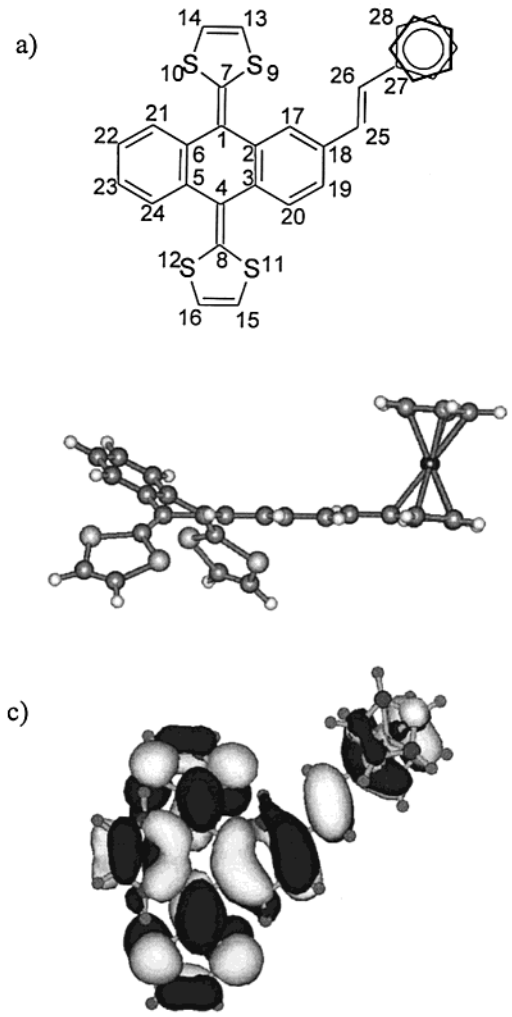

Figure 11. (a) Minimum energy conformations calculated by ZINDO1 for compound **16a**. An aleatory atom numbering is used in the text (top). (b) Butterfly shaped minimum-energy conformation calculated for **16a** showing the planarity of the vinyl spacer with the ferrocene moiety (middle). (c) HOMO of compound **16a** (bottom).

Molecular Structure. To justify our electrochemical observations, the molecular geometry of compound **16a** has been optimized by using semiempirical calculations at the ZINDO1 level. This theoretical method has been used as an alternative to the previously used PM3 level, which has provided good agreement between theory and experiments in the exTTFs,[3a] due to the presence of the iron atom in the Fc moiety.

The minimum-energy conformation of compound **16a** is shown in Figure 11b. As expected, the exTTF moiety is highly distorted out of planarity as a consequence of the strong steric interactions between the peri hydrogens and the sulfur atoms (1.78 Å). To avoid these interactions, the molecule adopts a butterfly shape with the central ring in a boat conformation, which is in good agreement with the X-ray analysis of analogue compounds **4** (R = CH_3)[3a] and **6**.[7]

Distortions from planarity in these exTTFs has been described in terms of angles α and γ. Angle α corresponds to the angle formed by the benzene rings (the wings of the butterfly), and angle γ defines the tilting of the dithiole rings and is obtained as the supplement of the C7−C2−C6−C5 dihedral angle (Figure 11a). The calculated angles for the more favorable conformation of compound **16a** (α = 147.1° and γ = 30.4°) are in agreement with that calculated for other related structures (B3−P86/6-31G*: α = 142.1° and γ = 34.0°) [3d] and that found for compound **4** (R = CH_3) in the crystal.[3a]

Figure 11b also shows the planarity of the vinyl ferrocene moiety, forming a dihedral angle C18−C25−C26−C27 of 177.6°, with the benzene ring fused to the exTTF moiety (dihedral angle C17−C18−C25−C26 = 5.1° and C25−C26−C-27-C2 = 169.9°). These calculated data reveal that the two electroactive Fc and exTTF units are in conjugation through the vinyl spacer, thus supporting the electrochemical results. In addition, the HOMO of compound **16a** is presented in Figure 11c and shows that this orbital is delocalized over the whole molecule, with larger coefficients on the exTTF moiety, which perfectly supports the electrochemical findings, i.e., the first electrochemical oxidation process, if separation was observed such as for **16a**−**c** in CH_3CN or for **16a** in THF, should be based on the exTTF moiety.

Conclusions

The synthesis of novel Fc-π-exTTF multicomponent D−D molecular hybrids **16a**−**c** was accomplished by the Wittig−Horner reaction of the respective phosphonate esters (**15a**−**c**) with 2-(2-ferrocenylvinyl)-9,10-anthraquinone (**18**). Electrochemical studies of these new conjugated hybrids were performed under different conditions and found that the effects of solvent, temperature, scan rate and the working electrode were significant. Separation of the oxidation process of the exTTF moiety from that of Fc unit for all the species **16a**−**c** was achieved in CH_3CN and two well-behaved redox processes were observed involving two and one electrons, respectively. This separation allowed the observation of pronounced intramolecular electronic interactions between the two different electron donating units (D−D interactions) using electrochemistry. Semiempirical calculations strongly support the electrochemical findings. The main conclusions of the electrochemical properties for **16a**−**c** in CH_3CN are thus outlined as following:

(i) The electrochemical behavior of the hybrids essentially retain the redox characteristics of the constituents (exTTF and Fc), showing initial oxidation from the neutral to a dicationic (Fc-exTTF $\rightleftarrows$ Fc-exTTF^{2+}) and finally to a tricationic (Fc-exTTF^{2+} $\rightleftarrows$ Fc^{+}-exTTF^{2+}) state in two distinct steps.

(ii) The first two-electron oxidation process originates from the exTTF moiety rather than the Fc unit, in perfect agreement with the semiempirical calculation.

(iii) Careful analysis by either CV or OSWV and UV−vis indicates that intramolecular electronic interactions between the two different electron donating moieties

(27) (a) Batsanov, A. S.; Bryce, M. R.; Coffin, M. A.; Green, A.; Hester, R. E.; Howard, J. A. K.; Lednev, I. K.; Martín, N.; Moore, A. J.; Moore, J. N.; Ortí, E.; Sánchez, L.; Savirón, M.; Viruela, P. M.; Viruela, R.; Ye, T. Q. *Chem. Eur. J.* **1998**, *4*, 2580. (b) Bando, P.; Martín, N.; Segura, J. L.; Seoane, C.; Ortí, E.; Viruela, P. M.; Viruela, R.; Albert, A.; Cano, F. H. *J. Org. Chem.* **1994**, *59*, 4618. (c) Illescas, B.; Martín, N.; Segura, J. L.; Seoane, C.; Ortí, E.; Viruela, P. M.; Viruela, R. *J. Org. Chem.* **1995**, *60*, 5643. (d) Illescas, B.; Martín, N.; Segura, J. L.; Seoane, C.; Ortí, E.; Viruela, P. M.; Viruela, R. *J. Mater. Chem.* **1995**, *5*, 1563. For a recent review on molecules exhibiting photoinduced charge-transfer properties, see: Martín, N.; Seoane, C. in *Handbook of Organic Conductive Molecules and Polymers, Vol. 1* (Ed.: Nalwa, H. S.), Wiley: **1997**, p 2−82.

were observed both in the charged state upon successive electrochemical oxidations and in the neutral ground state.

(iv) The exTTF-based oxidation process can be interpreted as examples of electron transfer (ET) reactions with significant inner reorganization energies with the first ET having a larger barrier than the second,[28] resulting in the coalescence of the first and second electronic processes into a single two-electron oxidation wave from a highly distorted geometry in the neutral state to a planar, aromatic hydrocarbon skeleton in the dicationic state.[20] It is therefore anticipated that further fine-tuning of the molecular structure in the exTTF moiety will allow the discovery of systems in which the one-step, two-electron oxidation can be separated, thus advancing our understanding of both the structural control of ET reactivity and intramolecular electronic interactions. This will open a very interesting research field in the ET reaction and intramolecular D−D interactions.

Experimental Section

Electrochemistry. Cyclic voltammetry (CV) and Osteryoung square wave voltammetry (OSWV) were performed on a Windows-driven BAS 100W electrochemical analyzer at variable temperatures with a three-electrode configuration in different solvents containing the substrate (0.5−1.0 mmol dm^{-3}) and a supporting electrolyte. A platinum or gold (ø 1 mm) or glassy carbon (ø 3 mm) disk served as the working electrode, a platinum wire (ø 1 mm) and a commercial Ag/AgCl-3M NaCl aqueous electrode being the counter and the reference electrodes, respectively. Both the counter and the reference electrodes were directly immersed in the electrolyte solution. The surface of the working electrode was polished with commercial Alumina No. 1C with a particle size of 1.0 micron prior to use or each measurement if adsorption was significant. The solvents used were purified and dried according to standard procedures prior to use. Tetrabutylammonium hexafluorophosphate ($TBAPF_6$) (>99%) was recrystallized twice from ethanol and dried in a vacuum overnight prior to use and was employed as the supporting electrolyte in 0.1 mol dm^{-3} concentration. Solutions were stirred and deaerated by bubbling argon for a few minutes prior to each voltammetric measurement. Scan rate was generally ranging from 20 to 1000 mV s^{-1}. OSWVs were obtained using a sweep width of 25 mV, a frequency of 15 Hz, a step potential of 4 mV, a S. W. amplitude of 25 mV, and a quiet time of 2 s. *iR* compensation (100% in THF and CH_2Cl_2, 80−90% in CH_3CN) was performed before each CV and OSWV measurements.

Synthesis. 2-(2-Ferrocenylvinyl)-9,10-anthraquinone (18). Method A. To a suspension of the phosphonium bromide **17** (0.5 mmol) and ferrocenecarboxaldehyde **14** (0.5 mmol), 30 mL of CH_2Cl_2 and 4.6 mL of NaOH (1.0 M) aqueous solution was added under an argon atmosphere. An emerald-green color appeared and the solution was gently stirred until the green color of the phosphorane dissappeared. The organic layer was separated and washed with water (75 mL), dried and the solvent was removed under reduced pressure. The resulting mixture was then purified by silica gel chromatography using hexane/methylene dichloride (1:2 v/v) as the eluent and a violet solid isomeric mixture of *Z* and *E* isomers was obtained in a 5% yield.

Method B. To a solution of the phosphonium bromide **17** (0.5 mmol) in dry THF (10 mL) was dropwise added 0.3 mL of *n*-BuLi (1.6 M in hexane) under an argon atmosphere. The resulting solution was stirred under reflux for 30 min. A suspension of ferrocene carboxaldehyde **14** (1.0 mmol) in dry THF (10 mL) was then added and kept under these conditions overnight. The solvent was removed under reduced pressure and the residue washed with water (75 mL) and extracted with CH_2Cl_2 (3 × 75 mL). The organic layer was dried, and the solvent was removed under reduced pressure. The resulting solid was purified by silica gel chromatography using hexane/methylene dichloride (1:2 v/v) as the eluent and a violet solid isomeric mixture of *Z* and *E* isomers was obtained in 42% yield.

Method C. To a solution of the phosphonium bromide **17** (0.5 mmol) in toluene, potassium *tert*-butoxide (0.5 mmol) was added and the resulting solution was stirred under reflux for 30 min. A suspension of ferrocene carboxaldehyde **14** (0.5 mmol) in toluene (20 mL) was then added and kept under these conditions overnight. The solvent was removed under reduced pressure and the residue washed with water (75 mL) and extracted with CH_2Cl_2 (3 × 75 mL). The organic layer was dried and the solvent was removed under reduced pressure. The resulting solid was purified by silica gel chromatography using hexane:methylene dichloride (1:2 v/v) as the eluent and a violet solid (*E* isomer only) was obtained in 90% yield: mp 195−196 °C; ^{1}H NMR ($CDCl_3$, 300 MHz) δ 4.17 (5H, s), 4.38 (2H, m), 4.54 (2H, m), 6.79 (1H, d, J = 16.1 Hz), 7.22 (1H, d, J = 16.1 Hz), 7.75 (1H, m), 7.80 (2H, m), 8.25 (1H, d, J = 8.1 Hz), 8.32 (3H, m); ^{13}C NMR ($CDCl_3$, 75 MHz) δ 65.5, 68.1, 69.5, 69.9, 81.9, 123.7, 123.9, 127.1, 127.2, 128.1, 128.4, 128.6, 130.8, 131.5, 132.2, 132.4, 132.7, 133.8, 134.1, 143.8; FTIR (KBr) 3421, 2403, 1676, 1589, 1326, 1299, 962, 710 cm^{-1}; UV−vis/λ_{max} (nm, methanol) (log ϵ) 535 (3.64), 372 (4.12), 310 (4.42), 275 (4.45), 250 (4.51), 218 (4.46); FAB-MS *m/z* 418 (M^+, 100); HRMS *m/z* found 418.0657, calcd for $C_{26}H_{18}O_2Fe$ 418.0656.

General Procedure for the Synthesis of 16a−c. To a solution of the corresponding 1,3-dithiolylphosphonate **15a−c** (1.5 mmol) in dry THF (10 mL) was dropwise added 1.0 mL of *n*-BuLi (1.6 M in hexane) under an argon atmosphere. The resulting solution was stirred at −78 °C for 30 min. A suspension of **18** (0.3 mmol) in dry THF (10 mL) was then added and kept under these conditions for an additional 1 h and then at room-temperature overnight. The solvent was removed under reduced pressure and the residue washed with water (75 mL) and extracted with CH_2Cl_2 (3 × 75 mL). The organic layer was dried and the solvent was removed under reduced pressure. The resulting solid was purified by silica gel chromatography using hexane:methylene dichloride (1:2 v/v) as the eluent.

2-(2-Ferrocenylvinyl)-9,10-bis(1,3-dithiol-2-ylidene)-9,10-dihydroanthracene (16a): 62% yield; mp 249−251 °C; ^{1}H NMR ($CDCl_3$, 300 MHz) δ 6.31 (2H, d, J = 3.2 Hz), 6.32 (2H, d, J = 3.4 Hz), 4.14 (5H, s), 4.29 (2H, m), 4.48 (2H, m), 6.73 (1H, d, J = 16.1 Hz), 6.92 (1H, d, J = 15.9), 7.31 (3H, m), 7.68 (3H, m), 7.77 (1H, d, J = 1.7 Hz); ^{13}C NMR ($CDCl_3$, 75 MHz) δ 66.8, 67.0, 69.2, 83.4, 117.1, 117.2, 117.3, 122.1, 122.2, 123.6, 124.9, 125.3, 125.7, 125.9, 127.1, 133.9, 135.3, 135.4, 135.7, 135.8; FTIR (KBr) 3855, 3659, 2924, 1512, 1452, 800, 754, 642 cm^{-1}; UV−vis/λ_{max} (nm, CH_2Cl_2) 437, 423 (sh), 376, 320; FAB-MS *m/z* 590 (M^+, 100); HRMS *m/z* found 589.9956, calcd for $C_{32}H_{22}S_4Fe$ 589.9954. Anal. Calcd for $C_{32}H_{22}S_4Fe$: C, 65.08; H, 3.75; S, 21.71. Found: C, 64.04; H, 4.03; S, 21.26.

2-(2-Ferrocenylvinyl)-9,10-bis(4,5-dimethylthio-1,3-dithiol-2-ylidene)-9,10-dihydroanthracene (16b): 59% yield; mp 260−262 °C; ^{1}H NMR ($CDCl_3$, 300 MHz) δ 2.39 (12H, s), 4.15 (5H, s), 4.31 (2H, m), 4.50 (2H, s), 6.72 (1H, d, J = 16.3 Hz), 6.94 (1H, d, J = 16.1 Hz), 7.34 (3H, m); 7.54 (3H, m), 7.61 (1H, m); ^{13}C NMR ($CDCl_3$, 75 MHz) δ 19.1, 19.1, 19.2, 69.3, 83.2, 116.1, 119.3, 121.3, 121.9, 122.6, 123.7, 123.8, 125.3, 125.4, 125.6, 125.8, 125.9, 125.9, 126.3, 126.4, 127.7, 130.9, 133.0, 135.1, 136.1; FTIR (KBr) 3437, 2918, 2852, 1533, 1497, 1452, 1419, 953, 823, 756, 640, 607 cm^{-1}; UV−vis/λ_{max} (nm, CH_2Cl_2) 446, 424 (sh), 381, 324; FAB-MS *m/z* 774 (M^+, 100%); HRMS *m/z* found 773.9462, calcd for $C_{36}H_{30}S_8Fe$ 773.9462. Anal. Calcd for $C_{36}H_{30}S_8Fe$: C, 55.80; H, 3.90; S, 33.10. Found: C, 54.98; H, 4.07; S, 33.20.

2-(2-Ferrocenylvinyl)-9,10-bis(4,5-ethylenedithio-1,3-dithiol-2-ylidene)-9,10-dihydroanthracene (16c): 64% yield; mp 185−187 °C; ^{1}H NMR ($CDCl_3$, 300 MHz) δ 3.30 (8H, m), 4.15 (5H, s), 4.30 (2H, m), 4.50 (2H, m), 6.73 (1H, d, J = 16.1 Hz), 6.93 (1H, d, J = 16.1 Hz), 7.31 (1H, dd, J_1 = 3.1 Hz, J_2 = 5.6 Hz), 7.36 (1H, dd, J_1 = 1.7 Hz, J_2 = 8.3 Hz), 7.49 (4H, m), 7.72 (1H, ddd, J_1 = 1.7 Hz, J_2 = 7.3 Hz, J_3 = 13.4 Hz); ^{13}C

(28) Ryan, M. D. *J. Electrochem. Soc.* **1978**, *125*, 547.

NMR ($CDCl_3$, 75 MHz) δ 29.6, 66.8, 67.2, 69.2, 69.3, 83.2, 110.9, 111.0, 122.7, 123.7, 124.2, 124.3, 125.4, 125.6, 125.9, 126.3, 126.4, 127.8, 128.4, 128.6, 129.2, 129.7, 131.5, 132.2, 132.3, 133.0, 134.6, 134.6, 135.0, 136.2; FTIR (KBr) 3437, 2920, 2852, 1508, 1452, 1410, 814, 754, 640, 608 cm^{-1}; UV−vVis/ λ_{max} (nm, CH_2Cl_2) 455, 432 (sh), 395, 325; FAB-MS *m*/*z* 770 (M^+, 50%); HRMS *m*/*z* found 769.9153, calcd for $C_{36}H_{26}S_8Fe$ 769.9150. Anal. Calcd for $C_{32}H_{22}S_4Fe$: C, 56.09; H, 3.40; S, 33.27. Found: C, 55.44; H, 4.02; S, 32.64.

Acknowledgment. Financial support by the Fulbright Foundation (Project 99125) is gratefully acknowledged. I.P. and N.M. thank the DGES of Spain (Project PB98-0818), and S.-G.L. and L.E. greatly appreciate the National Science Foundation, grant CHE-9803088, for generous support of this work.

JO001149W